

YONGHAO LUO^{1*}, YANGSHENG ZHAO^{2*}**FIELD AND EXPERIMENTAL RESEARCH ON AIRFLOW VELOCITY BOUNDARY LAYER
IN COAL MINE ROADWAY**

There is an airflow velocity boundary layer near tunnel wall when the air is flowing in the underground coal mine. The thickness and distribution of the airflow velocity boundary layer could influence the discharge of harmful and toxic gases that enter the ventilating airflow through this flow interface. It may also have a major impact in coal mine gas explosion. The results of field measurements and simulation experimental data are used to research airflow velocity boundary layer in a flat walled mine roadway, which is considered in turn: as unsupported, I-steel sectioned arch or bolted and shot create supported cross section. By referenced to other literature studies that consider boundary layer characteristics and the analysis of on-site and experimental data sets we obtain the corresponding airflow velocity boundary layer characteristics for each of the supported roadway sections. The airflow velocity within the boundary layer increase is assumed to follow a logarithmic law given by the expression: $u = a \ln(x) + b$. It is concluded that the thickness of the airflow velocity boundary layer is observed to significantly decrease with the airflow center velocity and to increase with roadway wall roughness. The airflow velocity distribution is found to be described by the equation: $u = (m_1v + n_1)\ln(d) + m_2v + n_2$, for the three types coal mine tunnel taking into account the influence of center airflow velocity.

Keywords: Coal mine roadway; Airflow velocity boundary layer; Mine measurement; Wind tunnel simulation; Supporting method; Logarithm distribution

1. Introduction

Boundary layer means a thin flow layer in high Reynolds number flow close to the object surface that the flow viscous force can not be neglected. Dave et al. (2013) defined the region

¹ TAIYUAN UNIVERSITY OF TECHNOLOGY, COLLEGE OF SAFETY AND EMERGENCY MANAGEMENT ENGINEERING, 030024, TAIYUAN, CHINA

² TAIYUAN UNIVERSITY OF TECHNOLOGY, COLLEGE OF MINING ENGINEERING, TAIYUAN, SHANXI PROVINCE 030024, CHINA

* Corresponding authors: luoyhmy@163.com; y-s-zhao@263.net



© 2020. The Author(s). This is an open-access article distributed under the terms of the Creative Commons Attribution-NonCommercial License (CC BY-NC 4.0, <https://creativecommons.org/licenses/by-nc/4.0/deed.en>) which permits the use, redistribution of the material in any medium or format, transforming and building upon the material, provided that the article is properly cited, the use is noncommercial, and no modifications or adaptations are made.

from boundary to speed reaches 99% of the free flow speed position as the boundary layer, which is the boundary layer thickness, in their fluid mechanics theory on calculating the boundary layer thickness accurately. General hydrodynamic literature were also considered as the distance from the boundary increases, the speed increases in a gradual manner and tends to the free flow speed. Therefore, between the boundary region and the main flow area is no clear dividing line. For convenience of description, the boundary layer thickness is defined as the distance that from the boundary to the position when the speed up to 99% of the free flow speed.

Boundary layer theory is widely applied and involving many fields. The research on the boundary layer has a significant impact on many fields, for example, wind-farm (Stevens et al., 2015; Dörenkämper et al., 2015), bacterial attachment (Chao et al., 2015), CO₂ corrosion of pipeline steels (Ko et al., 2015), the growth kinetics of carbon nanotube forests (Lee et al., 2015), aeronautics (Shi et al., 2015), and so on. Pal et al. (2017) investigated the diurnal cycle pattern of CO mixing ratio over a low mountaintop influenced by two different convective boundary layer (CBL) regimes (shallow and deep) and associated growth rates over the mountaintop. Skotniczny and Ostrogorski (2018) describes the results of an experiment determining the instantaneous values of velocity vector components of the air stream at selected spots of the boundary layer formed at the sidewalls of the mine heading in the LP type steel arch support.

In longwall development mining of coal seams, planning, optimizing and providing adequate ventilation are very important steps to eliminate the accumulation of explosive methane–air mixtures in the working environment (Karacan, 2007). The methane concentrations will be high if the wind velocity is low. Therefore, many studies have been carried out on underground mine air flow behaviors. Herdeen and Sullivan (1993) introduced computational fluid dynamics (CFDs) to investigate airflow ventilation in mines. Since then many scientists have used CFD to study mine airflow (Uchino & Inoue, 1997; Moloney & Lowndes, 1999; Wala et al., 2003; Yuan et al., 2006; Hargreaves & Lowndes, 2007).

The parameters of air stream flowing are also very important in describing the air flow behaviors. Therefore, Ligeza et al. (2009) presents an attempt of a numerical experiment the main goal of which was to determine the parameters of air stream flowing in the mine drift. Kumar et al. (2017) study the methane layering phenomenon and the effect of ventilation on dispersion of methane in underground coal mines at air velocities varying from 0.5 to 4.0 m/s. Geng et al. (2018) investigate dust dispersion driven by a hybrid ventilation system in an underground mine via a computational fluid dynamics (CFD) model.

In the wind velocity boundary layer the methane concentrations will be high and may be beyond statutory limits. Although conventional methods give satisfactory results when considering methane dilution, Toraño et al. (2009) proved that there may be some roadway zones in which methane concentration is higher than regulation values. Therefore we need to study the thickness and distribution of the airflow velocity boundary layer in coal mine roadway.

However, while wind velocity boundary layer has an important effect on the coal mine wind flow migration, the study on coal mine tunnel airflow velocity boundary layer has very few published papers. Because of airflow in coal mine flowing in limited space, the distribution of the airflow velocity boundary layer is different from the atmospheric boundary layer. In order to reveal the distribution of airflow velocity boundary layer in limited space in underground tunnel, this paper used field measurement and wind tunnel simulation methods to give a comparative study on the airflow velocity boundary layer.

2. Field research on airflow velocity boundary layer in coal mine tunnel

The field research was worked at Yuwu coal mine of Lu An Company in the province of Shanxi in the North of China. Yuwu coal mine's annual coal production is 10 million tons. The mine divided five mining area. The average thickness of coal seam is 6 m. The mining depth is 600 m. The cumulative length of the underground tunnel in ventilation system is 200 km.

There are three main types of roadway include I-steel supporting roadway, bolting and shotcreting supporting roadway and relatively smooth roadway reinforced by stone materials or made by hard intact rock roadway. The smoothing could influence the distribution of airflow in the coal mine roadway (Luo et al., 2015). The thickness of airflow velocity boundary layer in the coal mine roadway was influenced by the roughness of the wall of the roadway. Due to there is a significantly different roughness between different kinds of supporting roadway, we selected I-steel, bolting and shotcreting and flat wall three typical supporting roadways to measure the distribution of the airflow velocity in the airflow velocity boundary layer in coal mine roadway.

The testing methods for airflow velocity boundary layer included: (1) Test roadway selecting: choosing three roadways on each type in the boundary layer test. The testing roadways need have more than 500 m segment length and their size and shape need basically same. The maintenance time was chosen to avoid the trains and debris in the roadway. There were no large pipes flying in the roadway boundary, etc. (2) Test point arrangement: The measurement points were arranged in the middle of the roadway's height and measurement point's intervals were 5 cm within 1 m from the tunnel wall. (3) Test instrument: The anemometer's model is MAVS02. The accuracy of the anemometer is 0.01 m/s. 10 points were measured in each time and 3 minutes was set at each interval. The total test times were 10. (4) Finally, take the average of measuring results as the measuring point wind speed for analysis.

2.1. Field research on I-steel supporting roadway

I-steel supporting roadway is a common supporting roadway in coal mine and the roadway section is generally trapezoidal. The field research results on I-steel supporting roadway were introduced in following text (Connection roadway in N2103 as an example).

The roadway is located in the northwest of the mine, with roadway length 1009 m, roadway high 3.6 m, bottom width 4.78 m and middle position width 4.6 m. The roadway section is trapezoidal. The measurement location was 283 m apart from airflow entrance. The supporting beam's projection surface height is 12 cm, width is 9.5 cm and support spacing is 80 cm (shown in Fig. 1).

The airflow velocity in the roadway section center was 2.14 m/s and the roadway points' measured results were plotted in Figure 2. Figure 2 shows that with the increasing distance from the roadway wall, the airflow velocity increased rapidly at first, followed by a smooth transition growth and gradually stabilized close to the center of the roadway. The thickness of the airflow velocity boundary layer was 55.16 cm. According to the measured data analysis, the relationship of airflow velocity and distance in the boundary layer used logarithmic fitting curve and the correlation coefficient was 0.9854. The results indicated that the airflow velocity was logarithmic distribution in the boundary (shown in Fig. 2).

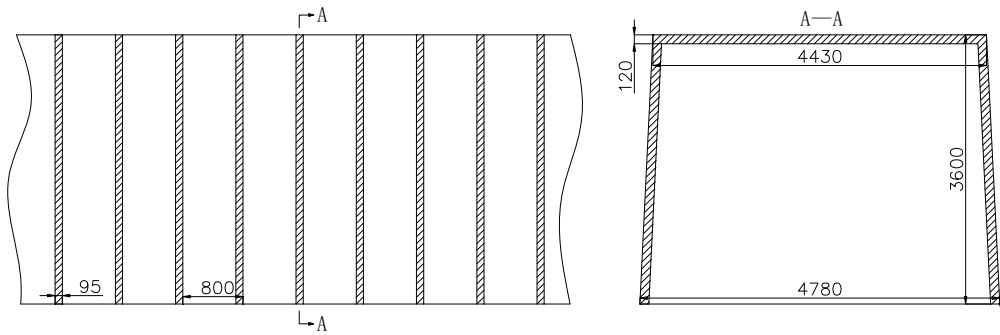


Fig. 1. Sectional drawing in Connection roadway in N2103

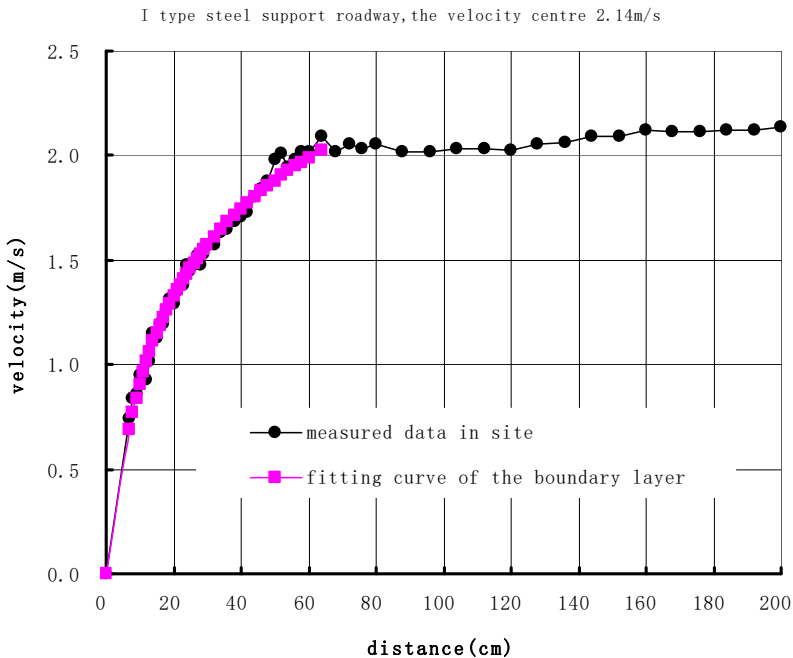


Fig. 2. Winds velocity in I type steel supporting roadway changing with distance from the boundary

2.2. Field research on bolting and shotcreting supporting roadway

The field research results on bolting and shotcreting roadway were introduced in following text (Northwest main ventilation roadway as an example). The roadway is located in the west of the mine, with roadway length 2147 m, roadway high 3.6 m and width 5 m. The roadway section is rectangle. The measurement location was 436 m apart from airflow entrance. The supporting bolting tray size is 15×15×0.8 (cm), bolting outcrop rod length is 12 cm and sup-

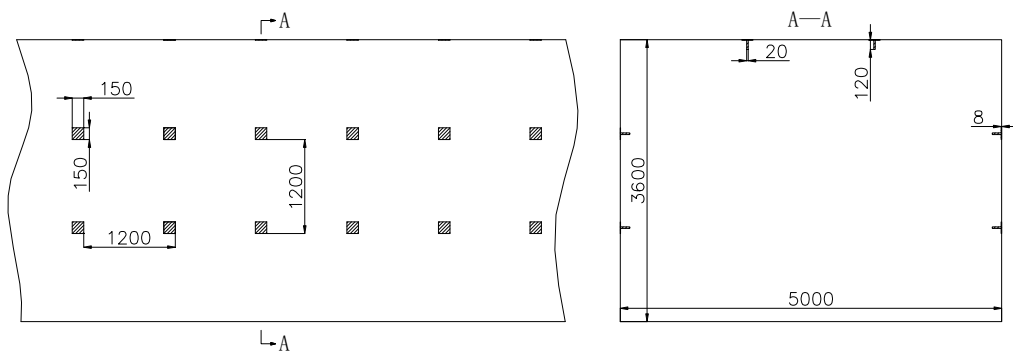


Fig. 3. Sectional drawing in Northwest main ventilation roadway

port spacing is 1.2 m. There were two rows of uniform supporting bolting both in roof and wall (shown in Fig. 3).

The airflow velocity in the roadway section center was 3.55 m/s and the roadway points' measured results were plotted in Figure 4. Figure 4 shows that with the increasing distance from the roadway wall, the airflow velocity increased rapidly at first and then gradually stabilized close to the center of the roadway. The thickness of the airflow velocity boundary layer was 30.87 cm. Compared with the I-steel supporting roadway the wind velocity in the bolting and shotcreting

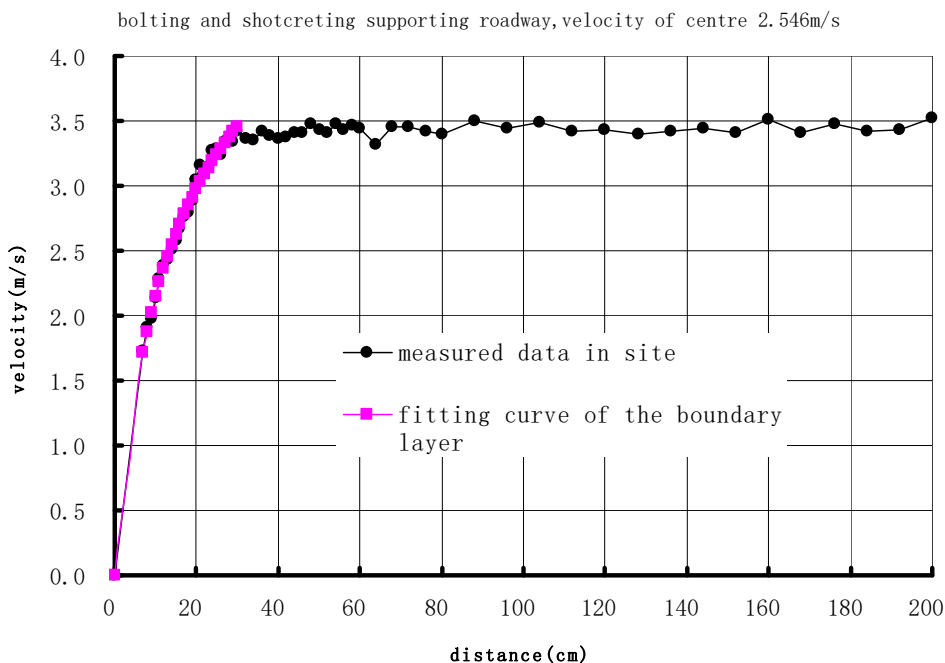


Fig. 4. Winds velocity in the bolting and shotcreting supporting roadway changing with distance from the boundary

supporting roadway in the growth segment was increased more rapidly. The airflow velocity was no longer had a significant increase after a certain stage and then fluctuation up and down in the value of certain airflow velocity.

The two figures were added after a certain stage is no longer a significant increase, and up and down fluctuations in the value of certain wind speed. The thickness of the airflow velocity boundary layer at bolting and shotcreting supporting roadway was thinner than I-steel supporting roadway.

Figure 4 shows the fitting curve of airflow velocity and distance in the boundary layer in bolting and shotcreting supporting roadway. The fitting curve is also logarithmic curve and the correlation coefficient was 0.9954. The results indicated that the airflow velocity was also logarithmic distribution in the boundary layer in bolting and shotcreting supporting roadway.

2.3. Field research on flat wall roadway

The field research results on flat wall roadway were introduced in following text (North cable car roadway as an example). The roadway is located in the middle of the mine, with roadway length 1642 m, roadway high 4.6 m and width 3.4 m. The roadway section is rectangle. The measurement location was 745 m apart from airflow entrance. The absolute roughness of wall is about 1.2 cm (shown in Fig. 5).

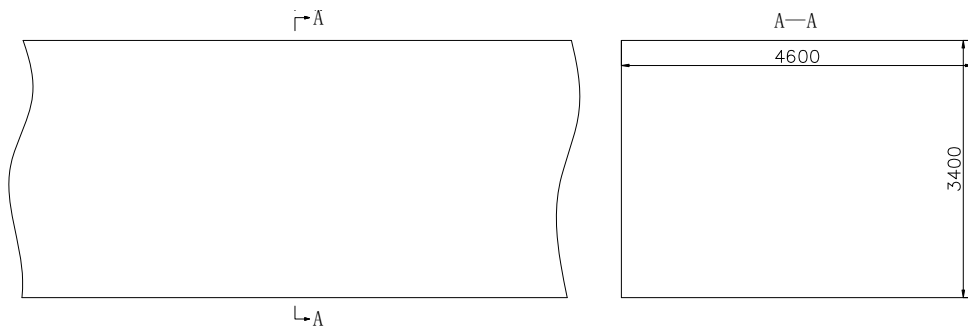


Fig. 5. Sectional drawing in North cable car roadway

The airflow velocity in the roadway section center was 4.60 m/s and the roadway points' measured results were plotted in Figure 6. The thickness of the airflow velocity boundary layer was 25.63 cm. Figure 6 shows that with the increasing distance from the roadway wall, the airflow velocity also increased rapidly at first and then gradually stabilized close to the center of the roadway.

Compared with the I-steel supporting roadway and bolting and shotcreting supporting roadway, the airflow velocity in the flat wall roadway in the growth segment was increased most rapidly. The airflow velocity was no longer had a significant increase after a certain stage and then fluctuation up and down in the value of certain airflow velocity in the three kinds of roadway. The thickness of the airflow velocity boundary layer at the flat wall roadway was thinnest among the three kinds of roadway.

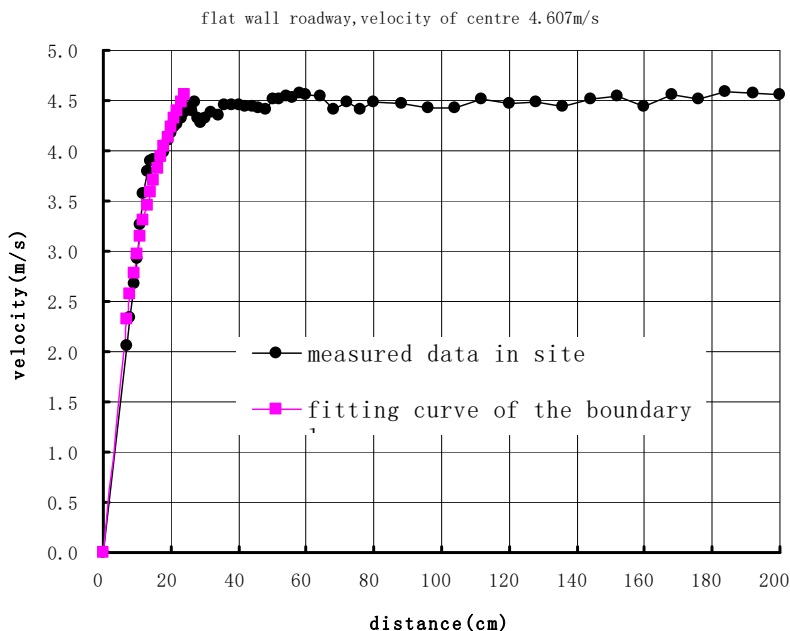


Fig. 6. Winds velocity in the flat wall roadway changing with distance from the boundary

Figure 6 shows the fitting curve of airflow velocity and distance in the boundary layer in flat wall roadway. The fitting curve is also logarithmic curve and the correlation coefficient was 0.9654.

The three types of roadway's center airflow velocity, airflow velocity boundary layer thickness, low airflow velocity region thickness (defined as $v < 0.8v_{centre}$) and the fitting results are summarized in Table 1. The fitting results of velocity and distance in I-steel supporting roadway, bolting and shotcreting supporting roadway and flat wall roadway show that the airflow velocity increases with the distance from the wall logarithmically ($u = a \ln(x) + b$, a and b are constants) in the boundary layer. The correlation coefficients were all more than 0.96. We can see that the a value is increased sequentially, the b value is decreased sequentially and the b absolute value is increased sequentially in I-steel supporting roadway, bolting and shotcreting supporting roadway and flat wall roadway.

TABLE 1

The airflow velocity boundary layer thickness, low airflow velocity region thickness and fitting parameters in three different supporting ways and center airflow velocities

Supporting method	Center airflow velocity (m/s)	Airflow velocity boundary layer thickness (cm)	Low airflow velocity region thickness (cm)	Fitting function	Correlation coefficient
I-steel	2.14	55.16	40.14	$y = 0.6049 \ln(x) - 0.4872$	0.9927
Bolting and shotcreting	3.55	30.87	18.45	$y = 1.1977 \ln(x) - 0.6137$	0.9954
Flat wall	4.60	25.63	12.49	$y = 1.8079 \ln(x) - 1.1874$	0.9645

3. Simulation experiment on airflow velocity boundary layer in coal mine tunnel

The field research shows that the supporting methods and center airflow velocities have a significant impact in airflow velocity boundary layer thickness and low airflow velocity region thickness. However, the airflow velocity could not be changed in field research. Therefore, we need to have a simulation experiment on different kinds of roadways to study the boundary layer thickness and boundary layer velocity distribution in different center airflow velocities in the roadway. Multiple repetitive experiments could also make the results more reliable.

3.1. Experimental method

- 1) We used underground engineering simulation tunnel (shown in Fig. 7) developed by Taiyuan University of Technology to have a simulation experiment. The section of tunnel is rectangle with length 20 m, high 1 m and width 1 m. The linear geometric ratio



Fig. 7. Pictures of underground engineering simulation tunnel. a) Picture of engineering simulation tunnel, b) I-steel simulation supporting roadway, c) Test measuring points of airflow velocity in boundary layer

- of simulation tunnel and field roadway is 1: 4-1: 5 approximately. The airflow velocity could be adjusted within the range of 0-20 m / s in the simulation tunnel. Luo and Zhao (2015) have given a detailed description on this tunnel.
- 2) The airflow velocity sensor's type is TSIMODEL1127. The sensors were arranged in the center and along the centerline level of the roadway with multi-point arrangement (shown in Fig. 7). The acquisition system's model is IFA300. This acquisition system could collect airflow velocity in real-time and continuous.
 - 3) Six center airflow velocities, 0.79, 2.02, 2.94, 3.63, 4.30 and 4.97 m / s were setting to test according to the actual range of airflow velocity in coal mine.
 - 4) The airflow velocity boundary layer in different supporting method roadways in coal mine was simulated by the simulation tunnel (shown in Fig. 7). The size and shape of model parts were arranged in the simulation tunnel according to the actual case in strict accordance with the actual geometry.
 - 5) The test was started after adjusting the roadway center airflow velocity reached on the set value and waiting for 20 minutes to system stable. The acquisition frequency of airflow velocity measurement was 10 times / Min. The acquisition time was 10 minutes. The airflow velocities in the data processing and analysis in the measurement points were the average results of 10 minutes' data.

3.2. Simulation experiment on I-steel supporting roadway

The size and shape of model parts for simulating I-steel supporting roadway were arranged in the simulation tunnel according to the actual case in strict accordance with the actual geometry. The test results (shown in Fig. 8) on boundary layer airflow velocities in different tunnel airflow velocities were obtained by acquisition system.

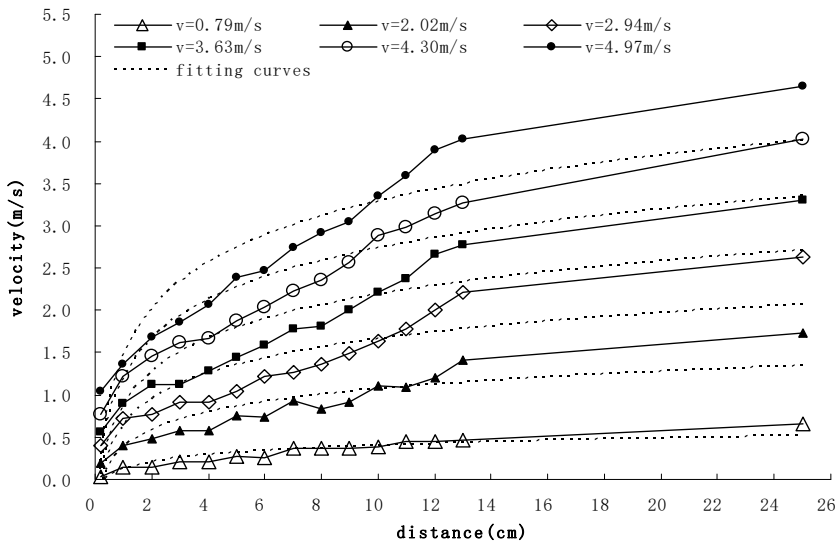


Fig. 8. Winds velocity in the I-steel supporting simulation roadway changing with distance from the roadway boundary

The test results in I-steel supporting roadway on boundary layer airflow velocities, in which the center airflow velocity was 0.79, 2.02, 2.94, 3.63, 4.30 and 4.97 m/s respectively, were shown in Figure 8. Figure 8 shows that with the increasing distance from the roadway wall, the airflow velocity increased rapidly near the wall, then gradually increased slowly. The relationship of airflow velocity and distance in the boundary layer used logarithmic fitting curve. The fitting curves were expressed by dotted line in Figure 8.

3.3. Simulation experiment on bolting and shotcreting supporting roadway

The size and shape of model parts for simulating bolting and shotcreting supporting roadway were arranged in the simulation tunnel according to the actual case in strict accordance with the actual geometry. The test results (shown in Fig. 9) on boundary layer airflow velocities in different tunnel airflow velocities were obtained by acquisition system.

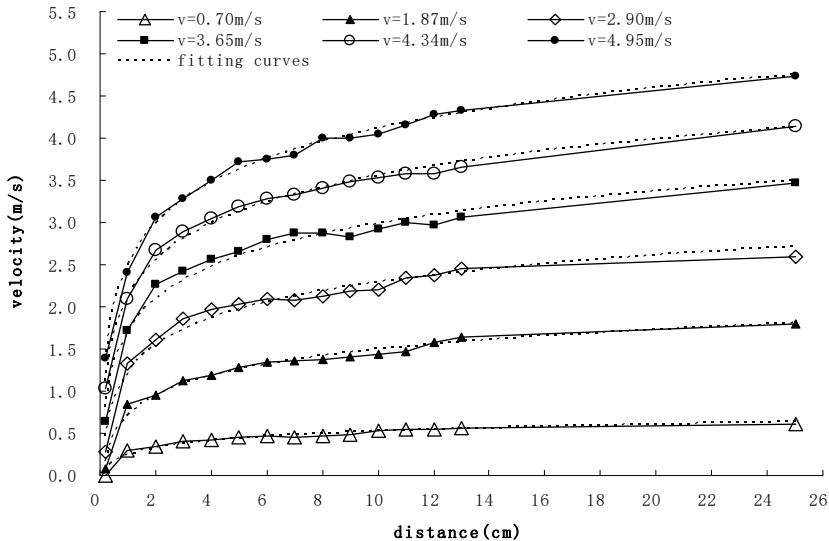


Fig. 9. Winds velocity in the bolting and shotcreting supporting simulation roadway changing with distance from the roadway boundary

The test results in bolting and shotcreting supporting roadway on boundary layer airflow velocities, in which the center airflow velocity was 0.70, 1.87, 2.90, 3.65, 4.34 and 4.95 m/s respectively, were shown in Figure 9. The relationship of airflow velocity and distance in the boundary layer used logarithmic fitting curve. The fitting curves were expressed by dotted line in Figure 9. Compared with the I-steel supporting roadway the wind velocity in the bolting and shotcreting supporting roadway near the wall was increased more rapidly and then increased more slowly. Compared with the I-steel supporting roadway the correlation coefficients in the bolting and shotcreting supporting roadway were higher.

3.4. Simulation experiment on flat wall roadway

There are many relatively smooth roadways without supporting parts on the wall in coal mine. These roadways were called flat wall roadway in this article. The wall was processed for simulating flat wall roadway in the simulation tunnel according to the actual case in strict accordance with the actual geometry. The test results (shown in Fig. 10) on boundary layer airflow velocities in different tunnel airflow velocities were obtained by acquisition system.

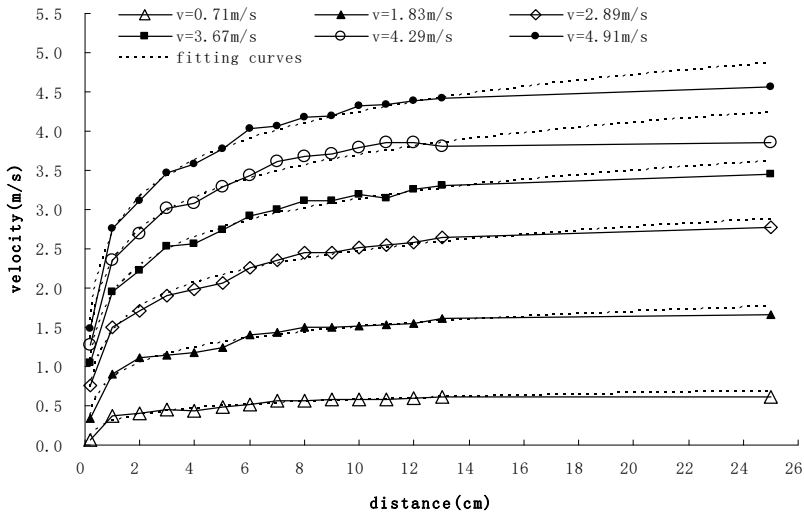


Fig. 10. Winds velocity in the flat wall simulation roadway changing with distance from the roadway boundary

The test results in flat wall roadway on boundary layer airflow velocities, in which the center airflow velocity was 0.71, 1.83, 2.89, 3.67, 4.29 and 4.91 m/s respectively, were shown in Figure 10. The relationship of airflow velocity and distance in the boundary layer used logarithmic fitting curve. The fitting curves were expressed by dotted line in Figure 10. Compared with the I-steel supporting roadway and the bolting and shotcreting supporting roadway the wind velocity in the flat wall roadway near the wall was increased more rapidly and then increased more slowly.

4. Airflow velocity boundary layer in different center airflow velocities in tunnel

The test results and fitting curves in I-steel supporting roadway, bolting and shotcreting supporting roadway and flat wall roadway on boundary layer airflow velocities were shown in Figure 8, Figure 9 and Figure 10, respectively. The fitting functions of airflow velocities in boundary layers in the simulation roadway with different center airflow velocity were shown in Table 2. Table 2 shows that the airflow velocity was logarithmic distribution in the boundary in three roadways though with different wall roughness and center airflow velocity. The correla-

tion coefficients of logarithmic laws and experimental results are very high. The fitting result in I-steel supporting roadway for the boundary layer was around 0.9. The fitting results in bolting and shotcreting supporting roadway and flat wall roadway for the boundary layer were both higher than 0.97.

TABLE 2

Fitting functions of winds in the simulation roadway changing with distance from the roadway boundary

Supporting method	Center airflow velocity (m/s)	Fitting function	Correlation coefficient
I-steel	0.79	$y = 0.1222\text{Ln}(x) + 0.1212$	0.9154
	2.02	$y = 0.2988\text{Ln}(x) + 0.3813$	0.8897
	2.94	$y = 0.4427\text{Ln}(x) + 0.6432$	0.8716
	3.63	$y = 0.5676\text{Ln}(x) + 0.8805$	0.8906
	4.30	$y = 0.6646\text{Ln}(x) + 1.2040$	0.9064
	4.97	$y = 0.7877\text{Ln}(x) + 1.4728$	0.9077
Bolting and shotcreting	0.70	$y = 0.1210\text{Ln}(x) + 0.2463$	0.9837
	1.87	$y = 0.3392\text{Ln}(x) + 0.7129$	0.9912
	2.90	$y = 0.4638\text{Ln}(x) + 1.2221$	0.9870
	3.65	$y = 0.5559\text{Ln}(x) + 1.7078$	0.9896
	4.34	$y = 0.6229\text{Ln}(x) + 2.1230$	0.9967
	4.95	$y = 0.6984\text{Ln}(x) + 2.5055$	0.9980
Flat wall	0.71	$y = 0.1179\text{Ln}(x) + 0.3046$	0.9762
	1.83	$y = 0.2833\text{Ln}(x) + 0.8509$	0.9878
	2.89	$y = 0.4425\text{Ln}(x) + 1.4523$	0.9937
	3.67	$y = 0.5260\text{Ln}(x) + 1.9214$	0.9942
	4.29	$y = 0.5930\text{Ln}(x) + 2.3315$	0.9841
	4.91	$y = 0.6761\text{Ln}(x) + 2.6893$	0.9920

Since the coal mine roadway section is small and with large tunnel wall roughness and great boundary layer thickness, it is always difficult to find airflow velocity region and point with velocity no less than 0.99 of central point velocity. Therefore, we define the region with velocity less than 0.8 of central point velocity as low airflow velocity region.

Table 2 shows that the coefficients a and b are different in the fitting functions of airflow velocities in boundary layers in the same roadway with different center airflow velocity. The coefficients k and b are also different in the fitting functions of airflow velocities in boundary layers with same center airflow velocity in the different roadway. The constants of k and b in the same roadway with different center airflow velocity were plotted in Fig. 11 and Fig. 12. We can see that there are good linear relationships between the constants of k and b with center airflow velocity. The correlation coefficients were 0.98 or more in linear fitting. Airflow velocity distribution functions in three coal mine tunnels with different supporting method taking into account the influence of center airflow velocity are summarized in Table 3. The second row in Table 3 gives the general expression of airflow velocity distribution function. The third, fourth and fifth row in Table 3 gives the expression of airflow velocity distribution function in I-steel supporting roadway, bolting and shotcreting supporting roadway and flat wall roadway, respectively. The mean of the parameters in Table 3 are list below.

- u — Airflow velocity within the boundary layer in simulate roadway, m/s;
- v — Airflow velocity in section center of simulated roadway, m/s;
- d — distance from the simulated roadway wall, m;
- m_1, n_1 — Characteristic constant of coefficient k ;
- m_2, n_2 — Characteristic constant of coefficient b .

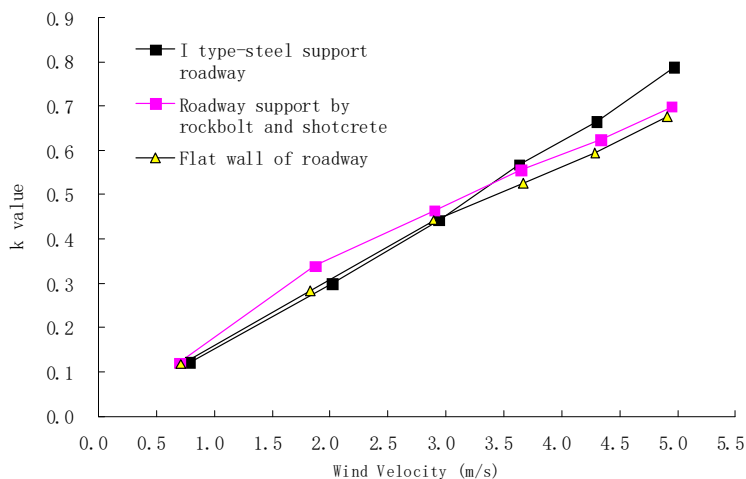


Fig. 11. The a value of boundary layer changing with winds velocity of roadway centre

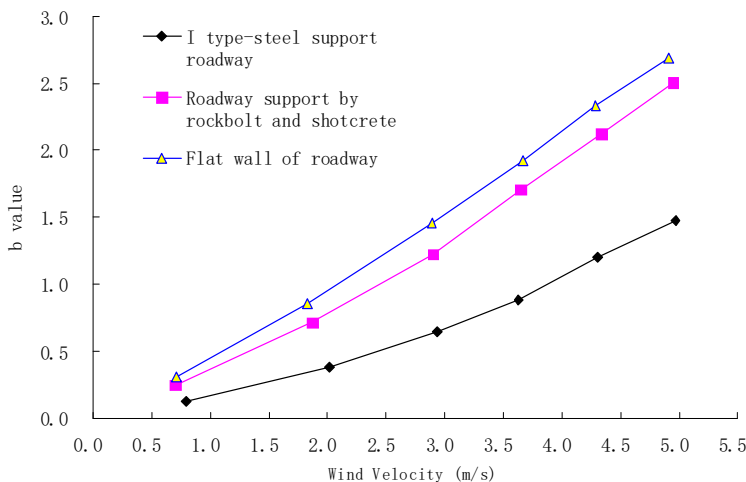


Fig. 12. The b value of boundary layer changing with winds velocity of roadway centre

Table 3 shows that the constant of m_1 is decreased with the roadway roughness and the constant of m_1 is increased with the roadway roughness. We need more field and experimental researches to find the relationship of constant n_1 and n_2 and roadway roughness.

TABLE 3

Functions of winds in the simulation roadway changing with distance and center wind velocity

Supporting method	Functions of winds in the airflow velocity boundary layer
All the methods	$u = (m_1v + n_1)\text{Ln}(d) + m_2v + n_2$
I-steel	$u = (0.1593v - 0.0147)\text{Ln}(d) + 0.3262v - 0.2302$
Bolting and shotcreting	$u = (0.1319v + 0.0620)\text{Ln}(d) + 0.5382v - 0.2316$
Flat wall	$u = (0.1315v + 0.0388)\text{Ln}(d) + 0.5740v - 0.1591$

We could obtain the function on airflow velocity distribution in boundary layer by measuring the related constants and using the law completed in this article. The function could provide guidance for the coal mine production safety.

5. Comparative analysis on confined space boundary layer and free space boundary layer

From the scientific level airflow velocity boundary layer can be divided into two categories, namely laminar boundary layer and turbulent boundary layer. From the physical visible level airflow velocity boundary layer can be divided into confined space boundary layer and free space boundary layer. The major study was on free space boundary layer such as about aircraft wing, missile, airflow in nature, and river boundary layer problems. There were also many achievements on this study. Kornilov (2015) has given a reviewed study on turbulent boundary layer on the status and future research directions. Degrazia et al. (2015) have given a studied on the turbulent boundary layer eddy diffusion problem. Lee (2015) investigated the changes of turbulent boundary layer on smooth surface and rough surface. Tse et al. (2015) investigated the tropical cyclone boundary layer and the research of the boundary layer thickness can be up to 1000 m with the highest wind speed exceeding 20 m/s. Ghate et al. (2011) investigated the vertical distribution of airflow velocity on atmospheric boundary layer in marine areas and the size of its research object was about 1000 m. Dong et al. (2007) proposed that the airflow velocity changing in the vertical direction is logarithmic law with and without carry the sand. Their research size was 1m vertically and airflow velocity up to 14 m/s.

There were also many researches on confined space boundary layer. Lengani and Simoni (2015) investigated the continuous and separation problem of airflow velocity boundary layer in low-pressure turbine blade under different turbulence intensity. Murena and Mele (2014) have given a research on the mass transfer efficiency in the middle of the street in atmospheric boundary layer in the field of air pollution. The boundary layer thickness was about 1.2 m with wind speed of 4 ± 2 m/s in the street with 18m in high and 6m in width. This is a class of semi-free space problem and has great difference with entirely confined space such as coal mine roadways and railway tunnels. Saha et al. (2011) proposed that the shear and friction near the wall increased with the airflow velocity and this could reduce the thickness of the boundary layer. Their measured results showed that the airflow velocity was logarithmic distribution in the boundary layer. These results are agreed with the conclusions of this article.

The confined space airflow velocity boundary layer is a very important and a very wide range issue. There are some related research reports with large gap of project type and scale but does not have the corresponding comparable. The research on airflow velocity boundary layer

in coal mine roadway has not published and the relevant research need be strengthened. These researches could guide a series of major issues on the ventilation in coal mine and underground space and preventing the disaster.

6. Conclusions

There is an airflow velocity boundary layer near tunnel wall when the air is flowing in the underground coal mine. The thickness and distribution of the airflow velocity boundary layer could influence the discharge of harmful and toxic gases. It also has a major impact in coal mine gas explosion. The field measurement and simulation experiment was used to research airflow velocity boundary layer and low airflow velocity region in coal mine tunnel. The following conclusions were obtained.

- 1) The thickness of airflow velocity boundary layer and low airflow velocity region is decreased sequentially in I-steel supporting roadway, bolting and shotcreting supporting roadway and flat wall roadway with the decreased of wall roughness. The airflow velocity increases with the distance from the wall logarithmically ($u = a \ln(x) + b$, a and b are constants related with wall roughness and center airflow velocity in roadway) in the boundary layer.
- 2) The thickness of the airflow velocity boundary layer decreases with airflow velocity in the roadway center significantly and increases with wall roughness in the roadway. There are good linear relationships between the constants of a and b with center airflow velocity. Airflow velocity distribution equation ($u = (m_1v + n_1)\ln(d) + m_2v + n_2$) in three types coal mine tunnel taking into account the influence of center airflow velocity was obtained.

Acknowledgments

This work was financed by the National Natural Science Foundation of China (No. 51404161). We would like to thank Yuwu Coal Company (China) for the access to their underground mines and for technical supporting on this study.

References

- Chao Z., Qiang L., Rong C., Xun Z., 2015. *Locomotion of bacteria in liquid flow and the boundary layer effect on bacterial attachment*. Biochemical & Biophysical Research Communications **461** (4), 671-676.
- Özgen Karacan C., 2007. *Development and application of reservoir models and artificial neural networks for optimizing ventilation air requirements in development mining of coal seams*. International Journal of Coal Geology **72** (3-4), 221-239.
- Dave N., Azih C., Yaras M.I., 2013. *A dns study on the effects of convex streamwise curvature on coherent structures in a temporally-developing turbulent boundary layer with supercritical water*. International Journal of Heat & Fluid Flow **44** (12), 635-643.
- Degrazia G.A., Maldaner S., Buske D., Rizza U., Buligon L., Cardoso V. et al., 2015. *Eddy diffusivities for the convective boundary layer derived from les spectral data*. Atmospheric Pollution Research, 6.
- Dong Z., Mu Q., Wang H., 2007. *Wind velocity profiles with a blowing sand boundary layer: theoretical simulation and experimental validation*. Journal of Geophysical Research Atmospheres **112** (D19), 216-229.
- Dörenkämper M., Witha B., Steinfeld G., Heinemann D., Kühn M., 2015. *The impact of stable atmospheric boundary layers on wind-turbine wakes within offshore wind farms*. Journal of Wind Engineering & Industrial Aerodynamics **144**, 146-153.

- Geng F., Luo G., Wang Y.C., Peng ZB., Hu S.Y., Zhang T.T., Chai, H.L., 2018. *Dust dispersion in a coal roadway driven by a hybrid ventilation system: A numerical study*. Process Safety And Environmental Protection **113**, 388-400.
- Ghate V.P., Miller M.A., Lynne D.P., 2011. *Vertical velocity structure of marine boundary layer trade wind cumulus clouds*. Journal of Geophysical Research **116** (D16), 971-978.
- Hargreaves D.M., Lowndes I.S., 2007. *The computational modeling of the ventilation flows within a rapid development drive*. Tunnelling and Underground Space Technology **22** (2), 150-160.
- Herdeen J., Sullivan P., 1993. *The application of CFD for evaluation of dust suppression and auxiliary ventilation systems used with continuous miners*. In: Proceeding of the 6th US Mine Ventilation Symposium, SME, Littleton, 293-297.
- Ko M., Ingham B., Laycock N., Williams D.E., 2015. *In situ synchrotron x-ray diffraction study of the effect of micro-structure and boundary layer conditions on CO₂ corrosion of pipeline steels*. Corrosion Science **90**, 192-201.
- Kornilov V.I., 2015. *Current state and prospects of researches on the control of turbulent boundary layer by air blowing*. Progress in Aerospace Sciences **76**, 1-23.
- Kumar P., Mishra D.P., Panigrahi D.C., Sahu P., 2015. *Numerical studies of ventilation effect on methane layering behaviour in underground coal mines*. Current Science **112**, 1873-1881.
- Lee J.H., 2015. *Turbulent boundary layer flow with a step change from smooth to rough surface*. International Journal of Heat & Fluid Flow **54**, 39-54.
- Lengani D., Simoni D., 2015. *Recognition of coherent structures in the boundary layer of a low-pressure-turbine blade for different free-stream turbulence intensity levels*. International Journal of Heat & Fluid Flow **54**, 1-13.
- Ligeza P., Poleszczyk E., Skotniczny P., 2009. *A three-dimensional modelling of the structure of flow parameter fields in mine drifts*. Archives of Mining Sciences **54**, 601-621.
- Luo Y., Zhao Y., 2015. *Wind tunnel simulation on wind speed distribution in coal mine roadways within different roughness*. Journal of Taiyuan University of Technology **02**, 235-237.
- Luo Y., Zhao Y., Wang Y., Chi M., Tang H., Wang S., 2015. *Distributions of airflow in four rectangular section roadways with different supporting methods in underground coal mines*. Tunnelling & Underground Space Technology **46**, 85-93.
- Moloney K.W., Lowndes I.S., 1999. *Comparison of measured underground air velocities and air flows simulated by computational fluid dynamics*. Trans. Inst. Min. Metall. (Sec. A: Min. Ind.) **108**, 105-114.
- Murena F., Mele B., Murena F., Mele B., 2014. *Effect of short-time variations of wind velocity on mass transfer rate between street canyons and the atmospheric boundary layer*. Atmospheric Pollution Research, 5.
- Pal S., Lee T.R., Wekker S.F.J.D., 2017. *A study of the combined impact of boundary layer height and near-surface meteorology to the CO diurnal cycle at a low mountaintop site using simultaneous lidar and in-situ observations*. Atmospheric Environment.
- Saha C.K., Wu W., Zhang G., Bjerg B., 2011. *Assessing effect of wind tunnel sizes on air velocity and concentration boundary layers and on ammonia emission estimation using computational fluid dynamics (CFD)*. Computers & Electronics in Agriculture **78** (1), 49-60.
- Shi Y., Bai J., Hua J., Yang T., 2015. *Numerical analysis and optimization of boundary layer suction on airfoils*. Chinese Journal of Aeronautics **02** (02), 357-367.
- Skotniczny P., Ostrogorski P., 2018. *Three-Dimensional Air Velocity Distributions in the Vicinity of a Mine Heading's Sidewall*. Archives of Mining Sciences **63**, 335-352.
- Stevens R., Gayme D., Meneveau C., 2015. *Coupled wake boundary layer model of wind-farms*. Journal of Renewable & Sustainable Energy **7** (2).
- Toraño J., Torno S., Menendez M., Gent M., Velasco J., 2009. *Models of methane behaviour in auxiliary ventilation of underground coal mining*. International Journal of Coal Geology **80** (1), 35-43.
- Tse K.T., Li S.W., Fung J.C.H., Chan P.W., 2015. *An information exchange framework between physical modeling and numerical simulation to advance tropical cyclone boundary layer predictions*. Journal of Wind Engineering & Industrial Aerodynamics **143**, 78-90.
- Uchino K., Inoue M., 1997. *Auxiliary ventilation at a heading of a face by a fan*. In: Proceeding of the 6th US Mine Ventilation Symposium, SME, Littleton, 493-496.
- Wala A., Jacob J., Brown J., Huang G., 2003. *New approaches to mine-face ventilation*. Mining Engineering **55** (3), 25-30.
- Yuan L., Smith A.C., Brune J.F., 2006. *Computational fluid dynamics study on ventilation flow paths in longwall gobs*. In: 11th US/North American Mine Ventilation Symposium, State College, PA, 591-598.